



# 1 Quantifying the drivers of surface ozone anomalies in the urban 2 areas over the Qinghai-Tibet Plateau

3 Hao Yin <sup>1,2,\*</sup>, Youwen Sun <sup>1,2,†,\*</sup>, Justus Notholt <sup>3</sup>, Mathias Palm <sup>3</sup>, and Cheng Liu <sup>2,4,5,6†</sup>

4 <sup>1</sup>Key Laboratory of Environmental Optics and Technology, Anhui Institute of Optics and Fine  
5 Mechanics, HFIPS, Chinese Academy of Sciences, Hefei 230031, China

6 <sup>2</sup>Department of Precision Machinery and Precision Instrumentation, University of Science and  
7 Technology of China, Hefei 230026, China

8 <sup>3</sup>University of Bremen, Institute of Environmental Physics, P. O. Box 330440, 28334 Bremen,  
9 Germany

10 <sup>4</sup>Anhui Province Key Laboratory of Polar Environment and Global Change, University of Science  
11 and Technology of China, Hefei 230026, China

12 <sup>5</sup>Center for Excellence in Regional Atmospheric Environment, Institute of Urban Environment,  
13 Chinese Academy of Sciences, Xiamen 361021, China

14 <sup>6</sup>Key Laboratory of Precision Scientific Instrumentation of Anhui Higher Education Institutes,  
15 University of Science and Technology of China, Hefei 230026, China

16 <sup>†</sup>Corresponding authors.

17 \*These authors contributed equally.

18 E-mail addresses: Youwen Sun (ywsun@aiofm.ac.cn) and Cheng Liu (chliu81@ustc.edu.cn)

## 19 Abstract

20 Improved knowledge of the chemistry and drivers of surface ozone over the Qinghai-Tibet  
21 Plateau (QTP) is significant for regulatory and control purposes in this high-altitude region in the  
22 Himalaya. In this study, we investigate the processes and drivers of surface ozone anomalies  
23 (defined as deviations of ozone levels relative to their seasonal means) between 2015 and 2020 in  
24 urban areas over the QTP. We separate quantitatively the contributions of anthropogenic emissions  
25 and meteorology to surface ozone anomalies by using the random forest (RF) machine learning  
26 model based meteorological normalization method. Diurnal and seasonal surface ozone anomalies  
27 over the QTP were mainly driven by meteorological conditions, such as temperature, planetary  
28 boundary layer height, surface incoming shortwave flux, downward transport velocity, and inter-  
29 annual anomalies were mainly driven by anthropogenic emission. Depending on region and  
30 measurement hour, diurnal surface ozone anomalies varied over  $-27.82 \mu\text{g}/\text{m}^3$  to  $37.11 \mu\text{g}/\text{m}^3$ , where  
31 meteorological and anthropogenic contributions varied over  $-33.88 \mu\text{g}/\text{m}^3$  to  $35.86 \mu\text{g}/\text{m}^3$  and  $-4.32$   
32  $\mu\text{g}/\text{m}^3$  to  $4.05 \mu\text{g}/\text{m}^3$ , respectively. Exceptional meteorology driven 97% of surface ozone  
33 nonattainment events from 2015 to 2020 in the urban areas over the QTP. Monthly averaged surface  
34 ozone anomalies varied with much smaller amplitudes than their diurnal anomalies, where  
35 meteorological and anthropogenic contributions varied over  $7.63 \mu\text{g}/\text{m}^3$  to  $55.61 \mu\text{g}/\text{m}^3$  and  $3.67$   
36  $\mu\text{g}/\text{m}^3$  to  $35.28 \mu\text{g}/\text{m}^3$  from 2015 to 2020, respectively. The inter-annual trends of surface ozone  
37 anomalies in Ngari, Lhasa, Naqu, Qamdo, Diqing, Haixi and Guoluo can be attributed to  
38 anthropogenic emissions by 95.77%, 96.30%, 97.83%, 82.30%, 99.26%, and 87.85%, and  
39 meteorology by 4.23%, 3.70%, 2.17%, 3.19%, 0.74%, and 12.15%, respectively. The inter-annual  
40 trends of surface ozone in other cities were fully driven by anthropogenic emission, where the  
41 increasing inter-annual trends would have larger values if not for the favorable meteorological  
42 conditions. This study can not only improve our knowledge with respect to spatiotemporal



1 variability of surface ozone but also provides valuable implication for ozone mitigation over the  
2 QTP.

### 3 **1. Introduction**

4 The Qinghai-Tibet Plateau (QTP) (27-45° N, 70-105° E), with an average altitude of 4000m  
5 above sea level (a.s.l), is the highest plateau in the world. It is known as the “Roof of the World”  
6 and the “Third Pole” (Qiu, 2008;Yang et al., 2013;Yin et al., 2017). The QTP has an area of  
7 approximately  $2.5 \times 10^6$  km<sup>2</sup> and accounts for about one quarter of China’s territory (Duo et al., 2018).  
8 The QTP is the source region of five major rivers in Asia, i.e., the Indus, Ganges, Brahmaputra,  
9 Yangtze, and Yellow rivers, which provide water resource to more than 1.4 billion people  
10 (Immerzeel et al., 2010). The QTP has been verified to be a critical region for regulating Asian  
11 monsoon climate and hydrological cycle, and it is thus an important ecological barrier of the whole  
12 Asia (Loewen et al., 2007;Yanai et al., 1992). The QTP has long been regarded as a pristine region  
13 due to its low population and industrial levels (Zhu et al., 2013). Due to its unique features of  
14 landform, ecosystem and monsoon circulation pattern, the QTP has been regarded as a sensitive  
15 region to anthropogenic impact, and is referred to as an important indicator of regional and global  
16 climate change (Qiu, 2008). The exogenous and local atmospheric pollutants are potential to  
17 accelerate the melting of glaciers, damage air quality, water sources, and grasslands, and threaten  
18 climate on regional and global scales (Yin et al., 2017;Yin et al., 2019c;Sun et al., 2021d;Pu et al.,  
19 2007;Kang et al., 2016). Therefore, improved knowledge of the evolutions and drivers of  
20 atmospheric pollutants in the QTP is of great importance for understanding local ecological situation  
21 and formulating regulatory policies.

22 Surface ozone (O<sub>3</sub>) is a major air pollutant that threatens human health and vegetation growth  
23 (Jerrett et al., 2009;Yin et al., 2021b). Surface ozone over the QTP is generated either from its local  
24 anthropogenic and natural precursors such as nitrogen oxides (NO<sub>x</sub>), volatile organic compounds  
25 (VOCs), and carbon monoxide (CO) via a chain of photochemical reactions or transported from  
26 long-distance regions by downwelling from the stratosphere. Surface ozone level is sensitive to local  
27 emissions, and meteorological conditions and transport. Meteorological conditions affect surface  
28 ozone level indirectly through changes in natural emissions of its precursors or directly via changes  
29 in wet and dry removal, dilution, chemical reaction rates, and transport flux. Emissions of air  
30 pollutants affect surface ozone level by perturbing the abundances of hydroperoxyl (HO<sub>2</sub>) and  
31 alkylperoxyl (RO<sub>2</sub>) radicals which are the key atmospheric constituents in formation of ozone. Some  
32 previous studies have presented the variability and analyzed qualitatively the drivers of surface  
33 ozone over the QTP at a specific site or region (Xu et al., 2016;Yin et al., 2019b;Yin et al., 2017;Zhu  
34 et al., 2004). However, none of these studies have quantitatively separated the contributions of  
35 anthropogenic emission and meteorology. Separation of anthropogenic and meteorological drivers  
36 is very important since it conveys us exactly which processes drive the observed ozone anomaly  
37 and therefore right conclusions can be made on whether an emission mitigation policy is effective.

38 Chemical transport models (CTMs) are widely used to evaluate the influences of meteorology  
39 and anthropogenic emission on atmospheric pollution levels (Hou et al., 2022;Sun et al., 2021a;Yin  
40 et al., 2020;Yin et al., 2019a). However, there are significant uncertainties in the emission  
41 inventories and in the models themselves, and shutting down an emission inventory in CTMs may  
42 cause large nonlinear effect, which inevitably influences the accuracy, performance and efficient of  
43 CTMs (Vu et al., 2019;Zhang et al., 2020). Mathematical and statistical models such as the multiple



1 linear regression (MLR) model and general additive models (GAMs) have also been used in many  
2 studies to quantify the influence of meteorological factors (Li et al., 2019; Li et al., 2020; Yin et al.,  
3 2021a; Yin et al., 2022; Zhai et al., 2019).

4 Machine learning (ML) is a well-known field that has been developing rapidly in recent years.  
5 Machine learning is a fusion of statistics, data science, and computing which experiences use across  
6 a very wide range of applications (Grange et al., 2018). Unlike most ML models such as artificial  
7 neural networks which are hard to understand the working mechanisms, the random forest (RF)  
8 model is not a “black-box” method, its prediction process can be explained, investigated, and  
9 understood (Gardner and Dorling, 2001; Grange et al., 2018; Grange and Carslaw, 2019; Shi et al.,  
10 2021). Recently, RF model based meteorological normalization technique has been proposed and  
11 used to decouple the meteorological influence on atmospheric pollution. For example, Vu et al. (2019)  
12 have used this technique to demonstrate that the clean air action plan implemented in 2013 was  
13 highly effective in reducing the anthropogenic emissions and improving air quality in Beijing. Shi  
14 et al. (2021) have used this technique to quantitatively evaluate changes in ambient NO<sub>2</sub>, ozone, and  
15 PM<sub>2.5</sub> concentrations arising from these emission changes in 11 cities globally during the COVID-  
16 19 lockdowns.

17 In this study, we investigate the evolutions, implications, and drivers of surface ozone  
18 anomalies (defined as deviations of ozone levels relative to their seasonal means) from 2015 to 2020  
19 in the urban areas over the QTP. Compared with previous studies that focus on surface ozone over  
20 the QTP, this study involves in larger area and longer time span. Most importantly, this study  
21 separates quantitatively the contributions of anthropogenic emission and meteorology to surface  
22 ozone anomalies by using the RF model based meteorological normalization method. This study  
23 can not only improve our knowledge with respect to spatiotemporal variability of surface ozone but  
24 also provides valuable implication for ozone mitigation over the QTP. We introduce detailed  
25 descriptions of surface ozone and meteorological field dataset in section 2. The method for  
26 separating contributions of meteorology and anthropogenic emission is presented in section 3.  
27 Section 4 analyzes spatiotemporal variabilities of surface ozone from 2015 to 2020 in each city over  
28 the QTP. The performance of the RF model used for surface ozone prediction over the QTP is  
29 evaluated in Section 5. We discuss the implications and the drivers of surface ozone anomalies from  
30 2015 to 2020 in each city over the QTP in section 6. We conclude this study in section 7.

## 31 **2. Data sources**

### 32 **2.1 Surface ozone data**

33 The QTP covers an area of 2.5 million square meter and has a population of around 3 million,  
34 with most of them living in several cities. During the in depth study of the atmospheric chemistry  
35 over the Tibetan Plateau, @Tibet field campaign, ozone photochemistry and its roles in ozone  
36 budget are of great interests in both background atmosphere and in QTP urban areas. The former  
37 represents the influence of anthropogenic emission and cross boundary transport on the nature cycle  
38 of ozone in pristine atmosphere. The latter represents not only the upper limit of ozone  
39 photochemistry contribution to its budget, also a demanding knowledge for the sake of ozone  
40 pollution management. Hourly surface ozone data in the urban areas over the QTP are available  
41 from the China National Environmental Monitoring Center (CNMEC) network  
42 (<http://www.cnemc.cn/en/>, last access: November 26, 2021). The CNMEC network based ozone  
43 measurements have been widely used in many studies for evaluation of regional atmospheric



1 pollution and transport over China (Lu et al., 2021; Lu et al., 2019a; Lu et al., 2020; Sun et al.,  
2 2021c; Sun et al., 2021d; Yin et al., 2021a; Yin et al., 2021b; Yin et al., 2022). The CNEMC network  
3 has deployed 33 measurement sites in 12 cities over the QTP (Table 1). The number of measurement  
4 sites in each city varies from 1 to 6. All surface ozone time series at each measurement site are  
5 provided by active differential absorption ultraviolet (UV) analyzers. For all the 33 measurement  
6 sites, hourly surface ozone data are available since 2015. We first removed unreliable measurements  
7 at all measurement sites in each city by using the filter criteria following our previous studies (Lu  
8 et al., 2018; Lu et al., 2020; Sun et al., 2021b; Sun et al., 2021d; Yin et al., 2021a; Yin et al., 2021b),  
9 then averaged all measurements in each city to generate a city representative dataset. All  
10 investigations in this study are performed on such city representative basis.

11 As illustrated in Figure 1, the QTP (Latitude range:  $26^{\circ}00' \sim 39^{\circ}47'$ , Longitude range:  $73^{\circ}19'$   
12  $\sim 104^{\circ}47'$ ) covers the Kunlun Mountain, the A-erh-chin Mountain and the Qilian Mountain in the  
13 north, the Pamir Plateau and the Karakorum Mountains in the west, the Himalayas in the south, and  
14 the Qinling Mountains and the Loess Plateau in the east. These 12 cities are the most populated  
15 areas over the QTP. All these cities except Aba and Diqing are located in Tibet or Qinghai provinces.  
16 Aba and Diqing are in Sichuan and Yunnan provinces, respectively. The area of these cities ranges  
17 from 7.7 to 430 thousand  $\text{km}^2$ , the altitude ranges from 2.3 to 4.8 km a.s.l., and the population ranges  
18 from 0.12 to 2.47 million. The residents within the 12 cities are about 3.85 million account for about  
19 51% of population over the QTP.

## 20 2.2 Meteorological data

21 Meteorological fields used in this study are from the Modern-Era Retrospective analysis for  
22 Research and Applications Version 2 (MERRA-2) dataset (Gelaro et al., 2017). The MERRA-2  
23 dataset is produced by the NASA Global Modeling and Assimilation Office and it can provide time  
24 series of many meteorological variables with a spatial resolution of  $0.5^{\circ} \times 0.625^{\circ}$  (The NASA Global  
25 Modeling and Assimilation Office (GMAO), 2022). The boundary layer height and surface  
26 meteorological variables are available per hour and other meteorological variables are available  
27 every 3 hours. It has been verified that the MERRA-2 meteorological fields over Chinese weather  
28 stations are in good agreement with the observations (Carvalho, 2019; Kishore Kumar et al.,  
29 2015; Song et al., 2018; Zhou et al., 2017). This MERRA-2 dataset has been extensively used in  
30 evaluations of regional atmospheric pollution formation and transport over China (Li et al., 2019; Li  
31 et al., 2020; Yin et al., 2022; Zhai et al., 2019).

## 32 3. Methodology

### 33 3.1 Quantifying seasonality and inter-annual variability

34 We quantify the seasonality and inter-annual variability of surface ozone from 2015 to 2020 in  
35 each city over the QTP by using a bootstrap resampling method. The principle of such bootstrap  
36 resampling method was described in detail in Gardiner et al. (2008). Many studies have verified the  
37 robustness of Gardiner's methodology in modeling the seasonality and inter-annual variabilities of  
38 a suite of atmospheric species (Sun et al., 2020; Sun et al., 2021a; Sun et al., 2021b; Sun et al.,  
39 2021d; Sun et al., 2018). In this study, we used a second Fourier series plus a linear function to fit  
40 surface ozone monthly mean time series from 2015 to 2020 over the QTP. The usage of  
41 measurements on monthly basis can improve the fitting correlation and lower the regression residual.  
42 As a result, the relationship between the measured and bootstrap resampled surface ozone monthly



1 mean time series can be expressed as,

$$2 \quad V(t, \mathbf{b}) = b_0 + b_1 t + b_2 \cos\left(\frac{2\pi t}{12}\right) + b_3 \sin\left(\frac{2\pi t}{12}\right) + b_4 \cos\left(\frac{4\pi t}{12}\right) + b_5 \sin\left(\frac{4\pi t}{12}\right) \quad (1)$$

$$3 \quad F(t, a, \mathbf{b}) = V(t, \mathbf{b}) + \varepsilon(t) \quad (2)$$

4 where  $F(t, a, \mathbf{b})$  and  $V(t, \mathbf{b})$  represent the measured and fitted surface ozone time series,  
5 respectively. The parameters  $b_0$ – $b_5$  contained in the vector  $\mathbf{b}$  are coefficients obtained from the  
6 bootstrap resampling regression with  $V(t, \mathbf{b})$ . The  $b_0$  is the intercept, and the  $b_1$  is the annual  
7 growth rate, and  $b_1/b_0$  is the inter-annual trend discussed below. The parameters  $b_2$ – $b_5$  describe  
8 the seasonality,  $t$  is the measurement time in month elapsed since January 2015, and  $\varepsilon(t)$  represents  
9 the residual between the measurements and the fitting results. The autocorrelation in the residual  
10 can increase the uncertainty in calculation of inter-annual trend. In this study, we have followed the  
11 procedure of Santer et al. (2008) and included the uncertainty arising from the autocorrelation in the  
12 residual.

### 13 **3.2 Random Forest (RF) model**

14 We have established a decision tree based random forest (RF) machine learning model to  
15 describe the relationships between hourly surface ozone concentrations (response variables) and  
16 their potential driving factors (predictive variables) in the urban areas over the QTP. As summarized  
17 in Table 2, predictive variables used in this study include time variables such as year 2015 to 2020,  
18 month 1 to 12, day of the year from 1 to 365, hour of the day from 0 to 23, and meteorological  
19 parameters such as wind, temperature, pressure, cloud fraction, rainfall, vertical transport, radiation  
20 and relative humidity. These time variables were selected as proxies for emissions since pollutant  
21 emissions vary by the time of day, day of the week, and season (Grange et al., 2018).

22 The detailed descriptions of RF machine learning model can be found in Breiman (2001).  
23 Briefly, the RF model is an ensemble model consisting of hundreds of individual decision tree  
24 models. Each individual decision tree model uses a bootstrap aggregating algorithm to randomly  
25 sample response variables and their predictive variables with a replacement from a training dataset.  
26 In this study, a single regression decision tree is grown in different decision rules based on the best  
27 fitting between surface ozone measurements and their predictive variables. The predictive variables  
28 are selected randomly to give the best split for each tree node. The predicted surface ozone  
29 concentrations are given by the final decision as the outcome of the weighted average of all  
30 individual decision trees. By averaging all predictions from bootstrap samples, the bagging process  
31 decreases variance and thus helps the model to minimize overfitting.

32 As shown in Figure 2, the whole dataset was randomly divided into (1) a training dataset to  
33 establish the random forest model and (2) a testing dataset (not included in model training) to  
34 evaluate the model performance. The training dataset was randomly selected from 70 % of the whole  
35 data and the remaining 30% was taken as the testing dataset. The hyperparameters for the RF model  
36 in this study were configured following those in Vu et al. (2019) and Shi et al. (2021) and are  
37 summarized as follows: the maximum tree of a forest is 300 ( $n_{\text{tree}}=300$ ), the number of variables  
38 for splitting the decision tree is 4 ( $m_{\text{try}}=4$ ), and the minimum size of terminal nodes is 3  
39 ( $\text{min\_node\_size}=3$ ). Since the meteorological variables differ in units and magnitudes, which could  
40 lead to unstable performance of the model. Therefore, we uniformized all meteorological variables  
41 via equation (3) before using them in the RF model. This pre-processing procedure can also speed  
42 up the establishment of the RF model.



$$\mathbf{z}_k = \frac{x_k - \mathbf{u}_k}{\sigma_k} \quad (3)$$

where  $\mathbf{u}_k$  and  $\sigma_k$  are the average and  $1\sigma$  standard deviation (STD) of  $x_k$ , and  $\mathbf{z}_k$  is the pre-processed value for parameter  $x_k$ .

### 3.3 Separation of meteorological and anthropogenic contributions

In order to separate the contributions of meteorology and anthropogenic emission to surface ozone anomalies in each city over the QTP, we have decoupled meteorology driven anomalies by using the RF model based meteorological normalization method. The meteorological normalization method was first introduced by Grange et al. (2018) and improved by Vu et al. (2019) and Shi et al. (2021). To decouple the meteorological influence, we first generated a new input dataset of predictive variables, which includes original time variables and resampled meteorological variables ( $T_{\text{surface}}$ ,  $U_{10}$ ,  $V_{10}$ , PBLH, CLDT, PRECOT, OMEGA, SWGDN, QV, TROPH). Specifically, meteorological variables at a specific selected hour of a particular day in the input dataset were generated by randomly selecting from the meteorological data during 1980 to 2020 at that particular hour of different dates within a four-week period (i.e., 2 weeks before and 2 weeks after that selected date). For example, the new input meteorological data at 18:00, 15 February 2018, are randomly selected from the meteorological data at 18:00 on any date from 1 to 29 February of any year during 1980 to 2020. This selection process was repeated 1000 times to generate a final input dataset. The 1000 meteorological data were then fed to the RF model to predict surface ozone concentration. The 1000 predicted ozone concentrations were then averaged as equation (4) to calculate the final meteorological normalized concentration ( $O_{3,\text{dew}}$ ) for that particular hour, day, and year.

$$O_{3,\text{dew}} = \frac{1}{1000} \sum_{i=1}^{1000} O_{3,i,\text{pred}} \quad (4)$$

where  $O_{3,i,\text{pred}}$  is the surface ozone concentration predicted by using the  $i^{\text{th}}$  meteorological data randomly selected from the meteorological data at the specific selected hour on any date from 1 to 29 February of any year in 1980 to 2020.  $O_{3,\text{dew}}$  represents surface ozone concentration under the mean meteorological conditions at the specific selected hour between 1980 to 2020.

If the seasonal variabilities of anthropogenic emission and meteorology are constant over year, the variability of surface ozone can be exactly reproduced by the seasonality plus the intercept in equation (1), i.e., the annual growth rate of surface ozone and the fitting residual should be close to zero. But this is not realistic in real world. Any year-to-year difference in either anthropogenic emission or meteorology could result in anomalies. We calculate surface ozone anomalies ( $O_{3,\text{anomalies}}$ ) in each city over the QTP by subtracting their seasonal mean values ( $O_{3,\text{mean}}$ ) from all hourly surface ozone measurements ( $O_{3,\text{individual}}$ ) through equation (5) (Hakkarainen et al., 2019; Hakkarainen et al., 2016; Mustafa et al., 2021).

$$O_{3,\text{anomalies}} = O_{3,\text{individual}} - O_{3,\text{mean}} \quad (5)$$

where  $O_{3,\text{mean}}$  in each city are approximated by the seasonality plus the intercept described in equation (1). As a result, the difference  $O_{3,\text{meteo}}$  between  $O_{3,\text{individual}}$  and  $O_{3,\text{dew}}$  calculated as equation (6) is the portion of anomalies induced by changes in meteorology. The difference  $O_{3,\text{emis}}$  between  $O_{3,\text{anomalies}}$  and  $O_{3,\text{meteo}}$  calculated as equation (7) represents the portion of anomalies induced by changes in anthropogenic emission.

$$O_{3,\text{meteo}} = O_{3,\text{individual}} - O_{3,\text{dew}} \quad (6)$$

$$O_{3,\text{emis}} = O_{3,\text{anomalies}} - O_{3,\text{meteo}} \quad (7)$$



1 By applying the meteorological normalization method, we finally separate the contributions of  
2 meteorology and anthropogenic emissions to the surface ozone anomalies in each city over the QTP.  
3 Positive  $O_{3,meteo}$  and  $O_{3,emis}$  indicate that changes in meteorology and anthropogenic emission  
4 cause surface ozone concentration above their seasonal mean values, respectively. Similarly,  
5 negative  $O_{3,meteo}$  and  $O_{3,emis}$  indicate that changes in meteorology and anthropogenic emission  
6 cause surface ozone concentration below their seasonal mean values, respectively.

#### 7 **4. Variabilities of surface ozone over the QTP**

##### 8 **4.1 Overall ozone level**

9 Statistical summary and box plot of surface ozone concentration (units:  $\mu\text{g}/\text{m}^3$ ) in each city  
10 over the QTP from 2015 to 2020 are presented in Table S1 and Figure S1, respectively. The average  
11 of surface ozone between 2015 and 2020 in each city over the QTP varied over  $(50.67 \pm 29.57)$   
12  $\mu\text{g}/\text{m}^3$  to  $(90.38 \pm 28.83)$   $\mu\text{g}/\text{m}^3$ , and the median value varied over  $53.00$   $\mu\text{g}/\text{m}^3$  to  $90.00$   $\mu\text{g}/\text{m}^3$ . In  
13 comparison, the averages of surface ozone between 2015 and 2020 in the Beijing-Tianjin-Hebei  
14 (BTH), the Fenwei Plain (FWP), the Yangtze River Delta (YRD) and the Pearl River Delta (PRD) in  
15 densely populated and highly industrialized eastern China were  $140.76$   $\mu\text{g}/\text{m}^3$ ,  $132.16$   $\mu\text{g}/\text{m}^3$ ,  $125.09$   
16  $\mu\text{g}/\text{m}^3$  and  $119.82$   $\mu\text{g}/\text{m}^3$ , respectively. The average of surface ozone between 2011 and 2015 at the  
17 suburb Nam Co station in the southern-central of the QTP was  $(47.00 \pm 12.43)$   $\mu\text{g}/\text{m}^3$  (Yin et al.,  
18 2019b). As a result, surface ozone levels in the urban areas over the QTP are much lower than those  
19 in urban areas in eastern China but higher than those in the suburb areas over the QTP. Among all  
20 cities over the QTP, the highest and lowest surface ozone concentration occurs in Haixi and Aba,  
21 with mean values of  $(90.38 \pm 28.83)$   $\mu\text{g}/\text{m}^3$  and  $(50.67 \pm 28.83)$   $\mu\text{g}/\text{m}^3$ , respectively. Generally,  
22 surface ozone concentrations in Qinghai province are higher than those in Tibet province.

23 The ambient air quality standard issued by the Chinese government regularized that the  
24 critical value (Class 1 limit) for the maximum 8-hour average ozone level is  $160$   $\mu\text{g}/\text{m}^3$ . With this  
25 rule, we summarize the number of nonattainment day per year in each city over the QTP in Table  
26 S1. The number of nonattainment day per city and per year over the QTP is only 2 between 2015  
27 and 2020. Ozone nonattainment events over the QTP typically occur in spring or summer. In  
28 comparison, the number of nonattainment day per city and per year over the BTH, FWP, YRD and  
29 PRD are much larger, with values of 78, 36, 82 and 45 between 2015 and 2020, respectively, and  
30 all ozone nonattainment events over these regions occur in summer. The number of nonattainment  
31 day in Ngari in 2020, Lhasa in 2016 and 2017, Shannan in 2017 and 2018, Haixi in 2015 and 2019,  
32 and Xining in 2017 are 13, 10, 20, 12, 10, 14, 16, and 17 days, respectively. The number of  
33 nonattainment day in all other cities over the QTP are less than 10 days. Especially, surface ozone  
34 concentrations in Aba, Naqu, and Diqing in all years between 2015 and 2020 are less than the Class  
35 1 limit of  $160$   $\mu\text{g}/\text{m}^3$ . There are only 1 and 2 nonattainment days in Nyingchi and Qamdo between  
36 2015 and 2020, respectively.

##### 37 **4.2 Diurnal variability**

38 Diurnal cycles of surface ozone in each season and each city over the QTP are presented in  
39 Figure 3. Overall, diurnal cycle of surface ozone in each city over the QTP presents a unimodal  
40 pattern in all seasons. For all cities in all seasons, high levels of surface ozone occur in the daytime  
41 (9:00 to 20:00 LT) and low levels of surface ozone occur in the nighttime (21:00 to 08:00 LT). As  
42 seen from Figure 3, surface ozone levels usually increase over time starting at 8:00 to 11:00 LT in



1 the morning, reach the maximum values at 15:00 to 18:00 LT in the afternoon, and then decreases  
2 over time till the minimum values at 8:00 or 9:00 LT the next day.

3 The timings of the diurnal cycles in all cities over the QTP were shifted by 1 to 2 hours later in  
4 winter than those in the rest of the year, most likely due to the later time of sunrise. (Yin et al., 2017)  
5 also observed such shift in diurnal cycle at the suburb Nam Co station. The diurnal cycles of surface  
6 ozone in the urban areas over the QTP spanned a large range of  $-43.73\%$  to  $47.12\%$  depending on  
7 region, season, and measurement time. The minimum and maximum surface ozone levels in the  
8 urban areas over the QTP varied over  $(22.89 \pm 15.55) \mu\text{g}/\text{m}^3$  to  $(68.96 \pm 18.27) \mu\text{g}/\text{m}^3$  and  $(57.77 \pm$   
9  $21.56) \mu\text{g}/\text{m}^3$  to  $(102.08 \pm 15.14) \mu\text{g}/\text{m}^3$ , respectively. On average, surface ozone levels in the urban  
10 areas over the QTP have mean values of  $(72.41 \pm 33.83) \mu\text{g}/\text{m}^3$  during the daytime (08:00-19:00)  
11 and  $(60.89 \pm 32.25) \mu\text{g}/\text{m}^3$  during the evening (20:00-08:00). The diurnal cycles of surface ozone in  
12 all cities over the QTP are generally consistent with the results reported in eastern China and the  
13 suburb areas over the QTP (Yin et al., 2019b; Yin et al., 2017; Zhao et al., 2016; Shen et al., 2014).

#### 14 4.3 Seasonal variability

15 Monthly averaged time series of surface ozone in each city over the QTP between 2015 and  
16 2020 are shown in Figure 4. Surface ozone levels in all cities over the QTP showed pronounced  
17 seasonal features. Seasonal cycles of surface ozone in most cities present a unimodal pattern with a  
18 seasonal peak occurs around March-July and a seasonal trough occurs around October-December.  
19 Specifically, maximum surface ozone levels occur in spring over Diqing, Lhasa, Naqu, Nyingchi,  
20 Qamdo, Shannan, Shigatse, Aba, and occur in summer over Ngari, Xining, Guoluo, and Haixi;  
21 Minimum surface ozone levels in Nyingchi and Diqing occur in autumn, and in other cities occur  
22 in winter. The minimum and maximum surface ozone levels between 2015 and 2020 over the QTP  
23 varied over  $(29.21 \pm 19.03) \mu\text{g}/\text{m}^3$  to  $(60.45 \pm 31.35) \mu\text{g}/\text{m}^3$  and  $(71.25 \pm 26.53) \mu\text{g}/\text{m}^3$  to  $(112.46 \pm$   
24  $28.92) \mu\text{g}/\text{m}^3$ , respectively (Table S2). The peak-to-trough contrast in Diqing, Naqu, Nyingchi, and  
25 Aba were smaller than those in other cities. Due to regional deference in meteorology and  
26 anthropogenic emission, seasonal cycle of surface ozone in the urban areas over the QTP is regional  
27 dependent.

#### 28 4.4 Inter-annual variability

29 The inter-annual variability of surface ozone between 2015 and 2020 in each city over the QTP  
30 fitted by the bootstrap resampling method is presented in Figure 5 and summarized in Table S2.  
31 Generally, the measured and fitted surface ozone concentrations in each city over the QTP are in  
32 good agreement with a correlation coefficient (R) of 0.68–0.92 (Figure S2). The measured features  
33 in terms of seasonality and inter-annual variability can be reproduced by the bootstrap resampling  
34 model. However, due to the year-to-year deference in anthropogenic emission and meteorology,  
35 both inter-annual variability and fitting residual were not zero in all cities. The inter-annual trends  
36 in surface ozone level from 2015 to 2020 over the QTP spanned a large range of  $(-2.43 \pm 0.56)$   
37  $\mu\text{g}/\text{m}^3 \cdot \text{yr}^{-1}$  to  $(7.55 \pm 1.61) \mu\text{g}/\text{m}^3 \cdot \text{yr}^{-1}$ , indicating a regional representation of each dataset. The inter-  
38 annual trends of surface ozone levels in most cities including Diqing, Naqu, Ngari, Nyingchi,  
39 Shannan, Shigatse, Xining, Abzhou and Haixi showed positive trends. The largest increasing trends  
40 were presented in Diqing and Nagri, with values of  $(5.31 \pm 1.28) \mu\text{g}/\text{m}^3 \cdot \text{yr}^{-1}$  and  $(7.55 \pm 1.61)$   
41  $\mu\text{g}/\text{m}^3 \cdot \text{yr}^{-1}$ , respectively. In contrast, surface ozone levels in Lhasa, Qamdo and Guoluo presented  
42 negative trends, with values of  $(-1.62 \pm 0.76) \mu\text{g}/\text{m}^3 \cdot \text{yr}^{-1}$ ,  $(-2.43 \pm 0.56) \mu\text{g}/\text{m}^3 \cdot \text{yr}^{-1}$  and  $(-2.36 \pm 0.81)$



1  $\mu\text{g}/\text{m}^3\cdot\text{yr}^{-1}$ , respectively.

## 2 **5. Performance evaluation**

3 We evaluate the performance of the RF model in predicting hourly surface ozone level in each  
4 city over the QTP using the metrics of Pearson correlation coefficient ( $R$ ), the root means square  
5 error (RMSE), and the mean absolute error (MAE). They are commonly used metrics for evaluation  
6 of machine learning model predictions, and are defined as equations (8), (9), and (10), respectively.

$$7 \quad R = \frac{n \sum_{i=0}^n x_i y_i - \sum_{i=0}^n x_i \sum_{i=0}^n y_i}{\sqrt{n \sum_{i=0}^n x_i^2 - (\sum_{i=0}^n x_i)^2} \cdot \sqrt{n \sum_{i=0}^n y_i^2 - (\sum_{i=0}^n y_i)^2}} \quad (8)$$

$$8 \quad RMSE = \sqrt{\frac{\sum_{i=1}^n (x_i - y_i)^2}{n}} \quad (9)$$

$$9 \quad MAE = \frac{\sum_{i=1}^n |x_i - y_i|}{n} \quad (10)$$

10 where  $x_i$  and  $y_i$  are the  $i^{\text{th}}$  concurrent measured and predicted data pairs, respectively. The  $n$  is the  
11 number of measurements. The  $R$  value represents the fitting correlation between the measurements  
12 and predictions. The RMSE value measures the relative average difference between the  
13 measurements and predictions. The MAE value measures the absolute average difference between  
14 the measurements and predictions. The units of RMSE and MAE are same as the measured data,  
15 namely  $\mu\text{g}/\text{m}^3$ .

16 Comparisons between the model predictions and measurements for the testing data (not  
17 included in model training) in each city over the QTP are shown in Figure S3. Overall, the RF model  
18 predictions and surface ozone measurements are in good agreements, showing high  $R$  and low  
19 RMSE and MAE for testing dataset in each city over the QTP (Figure S3). Depending on cities, the  
20  $R$  values varied over 0.85 to 0.94, the RMSE over 10.24 to 17.55  $\mu\text{g}/\text{m}^3$ , and MAE over 7.32 to  
21 12.76  $\mu\text{g}/\text{m}^3$ . The  $R$ , RMSE, and MAE are independent of city and surface ozone level. The results  
22 affirm that our model performs very well in predicting surface ozone levels and variabilities in each  
23 city over the QTP.

24 We also investigate the importance of each input variable in the RF model for predicting surface  
25 ozone level in each city over the QTP. As shown in Figure S4, time information such as hour term  
26 (Hour), year term (Year) or seasonal term (Month) are the most important variables in the RF model  
27 predictions in all cities except Xining and Haixi where temperature term ( $T_{2m}$ ) is the most important  
28 variable. For all cities, the aggregate importance of time information is larger than 50%. In all cities  
29 over the QTP, the meteorological variables such as temperature ( $T_{2m}$ ), relative humidity (QV),  
30 Vertical pressure velocity (OMEGA) and Planetary boundary layer height (PBLH) play significant  
31 roles when explaining surface ozone concentrations. For other variables, although they are not  
32 decisive variables in the RF model predictions, they are not negligible in predicting surface ozone  
33 in all cities over the QTP. Although time information are the most important variables in the RF  
34 model predictions, they can be used very precisely, and thus the RF model to measurement  
35 discrepancy in all cities could be from other predictive variables rather than time information.

## 36 **6. Drivers of surface ozone anomalies**

### 37 **6.1 Diurnal scale**

38 Figure 6 presents diurnal cycles of surface ozone anomalies between 2015 and 2020 along with  
39 the meteorology-driven and anthropogenic-driven portions in each city over the QTP. In all cities,



1 the anthropogenic contributions are almost constant but the meteorological contributions show large  
2 variations throughout the day. Depending on region and measurement hour, diurnal surface ozone  
3 anomalies on average varied over  $-27.82 \mu\text{g}/\text{m}^3$  to  $37.11 \mu\text{g}/\text{m}^3$  between 2015 and 2020, where  
4 meteorological and anthropogenic contributions varied over  $-33.88 \mu\text{g}/\text{m}^3$  to  $35.86 \mu\text{g}/\text{m}^3$  and  $-4.32$   
5  $\mu\text{g}/\text{m}^3$  to  $4.05 \mu\text{g}/\text{m}^3$ , respectively. The least contrast between meteorological contribution and  
6 anthropogenic contribution occurs in Haixi. The diurnal cycles of meteorological contribution are  
7 consistent with those of surface ozone anomalies. High levels of meteorological contribution occur  
8 in the daytime (9:00 to 20:00 LT) and low levels of meteorological contributions occur in the  
9 nighttime. As a result, diurnal surface ozone anomalies in each city over the QTP were mainly driven  
10 by meteorology.

11 We further investigated the drivers of surface ozone nonattainment events from 2015 to 2020  
12 in each city over the QTP. All ozone nonattainment events were classified as meteorology-  
13 dominated or anthropogenic-dominated events according to which one has a larger contribution to  
14 the observed surface ozone nonattainment events. The statistical results are listed in Table S3.  
15 Except one day in Ngari in 2018, one day in Shigatse in 2016, and one day in Haixi in 2019 which  
16 were dominated by anthropogenic emission, all other surface ozone nonattainment events from 2015  
17 to 2020 over the QTP were dominated by meteorology. Exceptional meteorology driven 97% of  
18 surface ozone nonattainment events from 2015 to 2020 in the urban areas over the QTP. For the  
19 meteorology-dominated surface ozone nonattainment events, meteorological and anthropogenic  
20 contributions varied over  $32.85 \mu\text{g}/\text{m}^3$  to  $55.61 \mu\text{g}/\text{m}^3$  and  $3.67 \mu\text{g}/\text{m}^3$  to  $7.23 \mu\text{g}/\text{m}^3$ , respectively.  
21 For the anthropogenic-dominated surface ozone nonattainment events, meteorological and  
22 anthropogenic contributions varied over  $7.63 \mu\text{g}/\text{m}^3$  to  $10.53 \mu\text{g}/\text{m}^3$  and  $15.63 \mu\text{g}/\text{m}^3$  to  $35.28 \mu\text{g}/\text{m}^3$ ,  
23 respectively.

## 24 6.2 Seasonal scale

25 Figure 7 presents seasonal cycles of surface ozone anomalies between 2015 and 2020 along  
26 with the meteorology-driven and anthropogenic-driven portions in each city over the QTP. In all  
27 cities, the monthly averaged surface ozone anomalies between 2015 and 2020 varied with much  
28 smaller amplitudes than their diurnal anomalies. Noticeable anomalies include pronounced positive  
29 anomalies in December in Nagri, in May in Lhasa, Shannan, and Qamdo, in July in Haixi, in June  
30 in Guoluo, and negative anomalies in July in Lhasa, Nyingchi, and Guoluo. Both meteorological  
31 and anthropogenic contributions are regional dependent and show large variations throughout the  
32 year. Depending on region and month, meteorological and anthropogenic contributions varied over  
33  $-4.54 \mu\text{g}/\text{m}^3$  to  $3.31 \mu\text{g}/\text{m}^3$  and  $-2.67 \mu\text{g}/\text{m}^3$  to  $3.35 \mu\text{g}/\text{m}^3$  between 2015 and 2020, respectively.

34 Seasonal surface ozone anomalies between 2015 and 2020 in all cities over the QTP were  
35 mainly driven by meteorology. For example, meteorology caused decrements of  $3.05 \mu\text{g}/\text{m}^3$  in July  
36 and  $4.27 \mu\text{g}/\text{m}^3$  in September in Diqing, while anthropogenic emission caused increments of  $0.64$   
37  $\mu\text{g}/\text{m}^3$  and  $1.34 \mu\text{g}/\text{m}^3$  in respective months. Aggregately, we observed  $-2.41 \mu\text{g}/\text{m}^3$  and  $-2.89 \mu\text{g}/\text{m}^3$   
38 of seasonal surface ozone anomalies in July and September in Ngari, respectively. In all cities,  
39 seasonal cycles of meteorological contribution are more consistent with those of surface ozone  
40 anomalies over the QTP. In some cases, surface ozone anomalies would have larger values if not for  
41 the unfavorable meteorological conditions, e.g., surface ozone anomalies in June in Ngari, in  
42 December in Shannan, Guoluo and Aba.



### 1 6.3 Annual scale

2 Annual mean surface ozone anomalies between 2015 and 2020 along with meteorology-driven  
3 and anthropogenic-driven portions in each city over the QTP are presented in Figure 8. Surface  
4 ozone in Diqing, Naqu, Nagri, Haixi and Shannan show larger year to year variations than those in  
5 other cities. Annual mean surface ozone levels in Diqing, Naqu, Nagri and Haixi showed significant  
6 reductions of  $2.10 \mu\text{g}/\text{m}^3$ ,  $10.32 \mu\text{g}/\text{m}^3$ ,  $6.87 \mu\text{g}/\text{m}^3$ , and  $15.97 \mu\text{g}/\text{m}^3$ , respectively, Shannan showed  
7 an increment of  $9.12 \mu\text{g}/\text{m}^3$ , and other cities showed comparable values in 2016 relative to 2015.  
8 The largest year to year difference occurred in Ngari during 2016 to 2017, which has an increment  
9 of  $25.25 \mu\text{g}/\text{m}^3$ . The results show that anthropogenic contributions decreased by  $1.85 \mu\text{g}/\text{m}^3$ ,  $7.14$   
10  $\mu\text{g}/\text{m}^3$ ,  $5.65 \mu\text{g}/\text{m}^3$ , and  $15.98 \mu\text{g}/\text{m}^3$ , respectively, in Diqing, Naqu, Nagri, Haixi, and increased by  
11  $11.13 \mu\text{g}/\text{m}^3$  in Shannan in 2016 relative to 2015, and increased by  $20.85 \mu\text{g}/\text{m}^3$  in Ngari in 2017  
12 relative to 2016. As a result, all above reductions or increments in surface ozone level were mainly  
13 driven by anthropogenic emission. In contrast, surface ozone anomalies in Lhasa in 2017 and 2020,  
14 in Shigatse and Nyingchi in 2019 were mainly driven by meteorology.

15 Table S4 summarizes the inter-annual trends of surface ozone anomalies, meteorological and  
16 anthropogenic contributions from 2015 to 2020 in each city over the QTP. Except Guoluo, Qamdo  
17 and Lhasa which show decreasing trends, anthropogenic contributions in all other cities showed  
18 increasing trends from 2015 to 2020. With respect to meteorology contribution, Ngari, Naqu, Diqing  
19 and Haixi showed increasing trends from 2015 to 2020 and all other cities showed decreasing trends.  
20 The inter-annual trends of surface ozone anomalies in Ngari, Lhasa, Naqu, Qamdo, Diqing, Haixi  
21 and Guoluo can be attributed to anthropogenic emissions by 95.77%, 96.30%, 97.83%, 82.30%,  
22 99.26%, and 87.85%, and meteorology by 4.23%, 3.70%, 2.17%, 3.19%, 0.74%, and 12.15%,  
23 respectively. The inter-annual trends of surface ozone in other cities were fully driven by  
24 anthropogenic emission, where the increasing inter-annual trends would have larger values if not  
25 for the favorable meteorological conditions. As a result, the inter-annual trends of surface ozone  
26 anomalies in all cities over the QTP were dominated by anthropogenic emission.

### 27 6.4 Discussions

28 Typically, all cities over the QTP are formed at flat valleys with surrounding mountains rising  
29 to more than 5.0 km a.s.l., and keep continuous expansion and development over time. Inhibited by  
30 surrounding mountains, regional dependent emissions and mountain peak-valley meteorological  
31 systems result in regional representation of surface zone level and their drivers on diurnal, seasonal,  
32 inter-annual scales.

33 Correlations between  $O_{3,meteo}$  and each meteorological anomalies are summarized in Table  
34 S5. We find that all time scales of meteorology-driven surface ozone anomalies in each city are  
35 positively related with anomalies of temperature, planetary boundary layer height (PBLH), surface  
36 incoming shortwave flux (SWGDN), downward transport velocity at the PBLH (OMEGA), and  
37 tropopause height (TROPH). Among all these positive correlations, the correlations with PBLH,  
38 SWGDN and OMEGA in all cities are higher than those with TROPH. Since high temperature and  
39 SWGDN facilitate the formation of ozone via the increase in chemical reaction rates or biogenic  
40 emissions, the meteorology-driven surface ozone anomalies are consistent with the changes in  
41 temperature and SWGDN. Possible reasons for the ozone increases with the increase in PBLH  
42 include lower NO concentration at the urban surface due to the deep vertical mixing, which then  
43 limits ozone destruction and increases ozone concentrations (He et al., 2017), and more downward



1 transport of ozone from the free troposphere where the ozone concentration is higher than the near-  
2 surface concentration (Sun et al., 2009). Large OMEGA and high tropopause height also facilitate  
3 downward transport of stratospheric ozone, resulting in high surface ozone level. The QTP has been  
4 identified as a hot spot for stratospheric–tropospheric exchange (Cristofanelli et al., 2010;Škerlak  
5 et al., 2014) where the surface ozone is elevated from the baseline during the spring due to frequent  
6 stratospheric intrusions. Generally, surface ozone anomalies are negatively related with humidity,  
7 rainfall, and total cloud fraction in each city over the QTP. These wet meteorological conditions  
8 inhibit biogenic emissions, slow down ozone chemical production, and facilitate the ventilation of  
9 ozone and its precursors (Gong and Liao, 2019;Jiang et al., 2021;Lu et al., 2019a;Lu et al.,  
10 2019b;Ma et al., 2019), and therefore contribute to ozone decrease.

11 The  $U_{10m}$  and  $V_{10m}$  represent the metrics for evaluating the horizontal transport. In most of  
12 cities over QTP, noticeable ozone vs. horizontal wind correlations are observed, indicating that  
13 horizontal transport is an important contributor to surface ozone (Shen et al., 2014;Zhu et al., 2004).  
14 The QTP region, as a whole, is primarily regulated by the interplay of the Indian summer monsoon  
15 and the westerlies, and the atmospheric environment over QTP is heterogeneous. Mount Everest is  
16 representative of the Himalayas on the southern edge of the Tibetan Plateau and is close to South  
17 Asia where anthropogenic atmospheric pollution has been increasingly recognized as disturbing the  
18 high mountain regions (Decesari et al., 2010;Maione et al., 2011;Putero et al., 2014). In the northern  
19 QTP, including Xining, Haixi and Guoluo, is occasionally influenced by regional polluted air masses  
20 (Xue et al., 2011;Zhu et al., 2004), especially, the impacts of anthropogenic emissions from central  
21 and eastern China in the summer (Xue et al., 2011). For cities over the inland QTP, is distant from  
22 both South Asia and northwestern China; it has been found to be influenced by episodic long-range  
23 transport of air pollution from South Asia (Lüthi et al., 2015), evidenced by the study of aerosol and  
24 precipitation chemistry at these cities (Cong et al., 2010).

25 The monthly and annual averaged anthropogenic emissions of  $\text{NO}_x$  and VOCs in each city over  
26 the QTP extracted from the MEIC (Multi-resolution Emission Inventory for China) inventory  
27 between 2015 to 2017 are presented in Table S6-S9. Major anthropogenic emissions in each city  
28 over the QTP are from transport sector and residential sector including burning emissions of coal,  
29 post-harvest crop residue, yak dung and religious incense (Chen et al., 2009;Kang et al., 2016;Kang  
30 et al., 2019;Li et al., 2017). Overall, both monthly and annual averaged anthropogenic contributions  
31 agree well with the changes of  $\text{NO}_x$  and VOCs emissions in MEIC inventory (Table S6-S9).

## 32 7. Conclusions

33 In this study, we have investigated the evolutions, implications, and the drivers of surface ozone  
34 anomalies (defined as deviations of ozone levels relative to their seasonal means) between 2015 and  
35 2020 in the urban areas over the QTP. Diurnal, seasonal, and inter annual variabilities of surface  
36 ozone in 12 cities over the QTP are analyzed. The average of surface ozone between 2015 and 2020  
37 in each city over the QTP varied over  $(50.67 \pm 29.57) \mu\text{g}/\text{m}^3$  to  $(90.38 \pm 28.83) \mu\text{g}/\text{m}^3$ , and the median  
38 value varied over  $53.00 \mu\text{g}/\text{m}^3$  to  $90.00 \mu\text{g}/\text{m}^3$ . Overall, diurnal cycle of surface ozone in each city  
39 over the QTP presents a unimodal pattern in all seasons. For all cities in all seasons, high levels of  
40 surface ozone occur in the daytime (9:00 to 20:00 LT) and low levels of surface ozone occur in the  
41 nighttime (21:00 to 08:00 LT). Seasonal cycles of surface ozone in most cities present a unimodal  
42 pattern with a seasonal peak occurs around March-July and a seasonal trough occurs around  
43 October-December. The inter-annual trends in surface ozone level from 2015 to 2020 over the QTP



1 spanned a large range of  $(-2.43 \pm 0.56) \mu\text{g}/\text{m}^3 \cdot \text{yr}^{-1}$  to  $(7.55 \pm 1.61) \mu\text{g}/\text{m}^3 \cdot \text{yr}^{-1}$ , indicating a regional  
2 representation of each dataset.

3 We have established a RF regression model to describe the relationships between hourly  
4 surface ozone concentrations (response variables) and their potential driving factors (predictive  
5 variables) in the urban areas over the QTP. The RF model predictions and surface ozone  
6 measurements are in good agreement, showing high  $R$  and low RMSE and MAE in each city over  
7 the QTP. Depending on cities, the  $R$  values varied over 0.85 to 0.94, the RMSE over 10.24 to 17.55  
8  $\mu\text{g}/\text{m}^3$ , and MAE over 7.32 to 12.76  $\mu\text{g}/\text{m}^3$ . The  $R$ , RMSE, and MAE are independent of city and  
9 surface ozone level. The results affirm that our model performs very well in predicting surface ozone  
10 levels and variabilities in each city over the QTP.

11 We have separated quantitatively the contributions of anthropogenic emission and meteorology  
12 to surface ozone anomalies by using the RF model based meteorological normalization method.  
13 Diurnal and seasonal surface ozone anomalies over the QTP were mainly driven by meteorology,  
14 and inter-annual anomalies were mainly driven by anthropogenic emission. Depending on region  
15 and measurement hour, diurnal surface ozone anomalies varied over  $-30.55 \mu\text{g}/\text{m}^3$  to  $34.01 \mu\text{g}/\text{m}^3$   
16 between 2015 and 2020, where meteorological and anthropogenic contributions varied over  $-20.08$   
17  $\mu\text{g}/\text{m}^3$  to  $48.73 \mu\text{g}/\text{m}^3$  and  $-27.18 \mu\text{g}/\text{m}^3$  to  $1.92 \mu\text{g}/\text{m}^3$ , respectively. Unfavorable meteorology driven  
18 97% of surface ozone nonattainment events between 2015 and 2020 in the urban areas over the QTP.  
19 Monthly averaged surface ozone anomalies varied with much smaller amplitudes than their diurnal  
20 anomalies, where meteorological and anthropogenic contributions varied over  $7.63 \mu\text{g}/\text{m}^3$  to  $55.61$   
21  $\mu\text{g}/\text{m}^3$  and  $3.67 \mu\text{g}/\text{m}^3$  to  $35.28 \mu\text{g}/\text{m}^3$  between 2015 and 2020, respectively. The inter-annual trends  
22 of surface ozone anomalies in Ngari, Lhasa, Naqu, Qamdo, Diqing, Haixi and Guoluo can be  
23 attributed to anthropogenic emissions by 95.77%, 96.30%, 97.83%, 82.30%, 99.26%, and 87.85%,  
24 and meteorology by 4.23%, 3.70%, 2.17%, 3.19%, 0.74%, and 12.15%, respectively. The inter-  
25 annual trends of surface ozone anomalies in other cities were fully driven by anthropogenic emission,  
26 where the increasing inter-annual trends would have larger values if not for the favorable  
27 meteorological conditions. This study can not only improve our knowledge with respect to  
28 spatiotemporal variability of surface ozone but also provides valuable implication for ozone  
29 mitigation over the QTP.

30 **Code and data availability.** All other data are available on request of the corresponding author  
31 (Youwen Sun, ywsun@aiofm.ac.cn).

32 **Author contributions.** HY designed the study and wrote the paper. YS supervised and revised this  
33 paper. JN, MP, and CL provided constructive comments.

34 **Competing interests.** None.

35 **Acknowledgements.** This work is jointly supported by the Youth Innovation Promotion Association,  
36 CAS (No.2019434) and the Sino-German Mobility programme (M-0036) funded by the National  
37 Natural Science Foundation of China (NSFC) and Deutsche Forschungsgemeinschaft (DFG).

38



1 **Reference**

- 2 Breiman, L.: Random Forests, *Machine Learning*, 45, 5-32, 10.1023/A:1010933404324, 2001.
- 3 Carvalho, D.: An Assessment of NASA's GMAO MERRA-2 Reanalysis Surface Winds, *J Climate*, 32,  
4 8261-8281, 10.1175/JCLI-D-19-0199.1, 2019.
- 5 Chen, D., Wang, Y., McElroy, M. B., He, K., Yantosca, R. M., and Le Sager, P.: Regional CO pollution  
6 and export in China simulated by the high-resolution nested-grid GEOS-Chem model, *Atmos Chem*  
7 *Phys*, 9, 3825-3839, 2009.
- 8 Cong, Z., Kang, S., Zhang, Y., and Li, X.: Atmospheric wet deposition of trace elements to central Tibetan  
9 Plateau, *Applied Geochemistry*, 25, 1415-1421, <https://doi.org/10.1016/j.apgeochem.2010.06.011>,  
10 2010.
- 11 Cristofanelli, P., Bracci, A., Sprenger, M., Marinoni, A., Bonafè, U., Calzolari, F., Duchi, R., Laj, P.,  
12 Pichon, J. M., Roccatò, F., Venzac, H., Vuillemoz, E., and Bonasoni, P.: Tropospheric ozone  
13 variations at the Nepal Climate Observatory-Pyramid (Himalayas, 5079 m a.s.l.) and influence of  
14 deep stratospheric intrusion events, *Atmos. Chem. Phys.*, 10, 6537-6549, 10.5194/acp-10-6537-  
15 2010, 2010.
- 16 Decesari, S., Facchini, M. C., Carbone, C., Giulianelli, L., Rinaldi, M., Finessi, E., Fuzzi, S., Marinoni,  
17 A., Cristofanelli, P., Duchi, R., Bonasoni, P., Vuillemoz, E., Cozic, J., Jaffrezo, J. L., and Laj, P.:  
18 Chemical composition of PM<sub>10</sub> and PM<sub>1</sub> at the high-altitude Himalayan station Nepal Climate  
19 Observatory-Pyramid (NCO-P) (5079 m a.s.l.), *Atmos. Chem. Phys.*, 10, 4583-4596, 10.5194/acp-  
20 10-4583-2010, 2010.
- 21 Duo, B., Cui, L. L., Wang, Z. Z., Li, R., Zhang, L. W., Fu, H. B., Chen, J. M., Zhang, H. F., and Qiong,  
22 A.: Observations of atmospheric pollutants at Lhasa during 2014-2015: Pollution status and the  
23 influence of meteorological factors, *J Environ Sci*, 63, 28-42, 2018.
- 24 Gardiner, T., Forbes, A., de Maziere, M., Vigouroux, C., Mahieu, E., Demoulin, P., Velazco, V., Notholt,  
25 J., Blumenstock, T., Hase, F., Kramer, I., Sussmann, R., Stremme, W., Mellqvist, J., Strandberg, A.,  
26 Ellingsen, K., and Gauss, M.: Trend analysis of greenhouse gases over Europe measured by a  
27 network of ground-based remote FTIR instruments, *Atmos Chem Phys*, 8, 6719-6727, 2008.
- 28 Gardner, M., and Dorling, S.: Artificial Neural Network-Derived Trends in Daily Maximum Surface  
29 Ozone Concentrations, *Journal of the Air & Waste Management Association*, 51, 1202-1210,  
30 10.1080/10473289.2001.10464338, 2001.
- 31 Gelaro, R., McCarty, W., Suárez, M. J., Todling, R., Molod, A., Takacs, L., Randles, C. A., Darmenov,  
32 A., Bosilovich, M. G., Reichle, R., Wargan, K., Coy, L., Cullather, R., Draper, C., Akella, S.,  
33 Buchard, V., Conaty, A., da Silva, A. M., Gu, W., Gi-Kong, K., Koster, R., Lucchesi, R., Merkova,  
34 D., Nielsen, J. E., Partyka, G., Pawson, S., Putman, W., Rienecker, M., Schubert, S. D., Sienkiewicz,  
35 M., and Zhao, B.: The Modern-Era Retrospective Analysis for Research and Applications, Version  
36 2 (MERRA-2), *J Climate*, 30, 5419-5454, <http://dx.doi.org/10.1175/JCLI-D-16-0758.1>, 2017.
- 37 Gong, C., and Liao, H.: A typical weather pattern for ozone pollution events in North China, *Atmos.*  
38 *Chem. Phys.*, 19, 13725-13740, 10.5194/acp-19-13725-2019, 2019.
- 39 Grange, S. K., Carslaw, D. C., Lewis, A. C., Boleti, E., and Hueglin, C.: Random forest meteorological  
40 normalisation models for Swiss PM<sub>10</sub> trend analysis, *Atmos Chem Phys*, 18, 6223-6239, 2018.
- 41 Grange, S. K., and Carslaw, D. C.: Using meteorological normalisation to detect interventions in air  
42 quality time series, *Sci Total Environ*, 653, 578-588, 2019.
- 43 Hakkarainen, J., Ialongo, I., and Tamminen, J.: Direct space-based observations of anthropogenic CO<sub>2</sub>  
44 emission areas from OCO-2, *Geophys Res Lett*, 43, 11400-411406,



- 1 <https://doi.org/10.1002/2016GL070885>, 2016.
- 2 Hakkarainen, J., Ialongo, I., Maksyutov, S., and Crisp, D.: Analysis of Four Years of Global XCO<sub>2</sub>  
3 Anomalies as Seen by Orbiting Carbon Observatory-2, *Remote Sens-Basel*, 11,  
4 10.3390/rs11070850, 2019.
- 5 He, J., Gong, S., Yu, Y., Yu, L., Wu, L., Mao, H., Song, C., Zhao, S., Liu, H., Li, X., and Li, R.: Air  
6 pollution characteristics and their relation to meteorological conditions during 2014–2015 in major  
7 Chinese cities, *Environmental Pollution*, 223, 484-496,  
8 <https://doi.org/10.1016/j.envpol.2017.01.050>, 2017.
- 9 Hou, L. L., Dai, Q. L., Song, C. B., Liu, B. W., Guo, F. Z., Dai, T. J., Li, L. X., Liu, B. S., Bi, X. H.,  
10 Zhang, Y. F., and Feng, Y. C.: Revealing Drivers of Haze Pollution by Explainable Machine  
11 Learning, *Environ Sci Tech Let*, 9, 112-119, 2022.
- 12 Immerzeel, W. W., van Beek, L. P. H., and Bierkens, M. F. P.: Climate Change Will Affect the Asian  
13 Water Towers, *Science*, 328, 1382-1385, 2010.
- 14 Jerrett, M., Burnett, R. T., Pope, C. A., Ito, K., Thurston, G., Krewski, D., Shi, Y., Calle, E., and Thun,  
15 M.: Long-Term Ozone Exposure and Mortality, *New Engl J Med*, 360, 1085-1095,  
16 10.1056/NEJMoa0803894, 2009.
- 17 Jiang, Z., Li, J., Lu, X., Gong, C., Zhang, L., and Liao, H.: Impact of western Pacific subtropical high on  
18 ozone pollution over eastern China, *Atmos. Chem. Phys.*, 21, 2601-2613, 10.5194/acp-21-2601-  
19 2021, 2021.
- 20 Kang, S. C., Huang, J., Wang, F. Y., Zhang, Q. G., Zhang, Y. L., Li, C. L., Wang, L., Chen, P. F., Sharma,  
21 C. M., Li, Q., Sillanpaa, M., Hou, J. Z., Xu, B. Q., and Guo, J. M.: Atmospheric Mercury  
22 Depositional Chronology Reconstructed from Lake Sediments and Ice Core in the Himalayas and  
23 Tibetan Plateau, *Environmental Science & Technology*, 50, 2859-2869, 2016.
- 24 Kang, S. C., Zhang, Q. G., Qian, Y., Ji, Z. M., Li, C. L., Cong, Z. Y., Zhang, Y. L., Guo, J. M., Du, W. T.,  
25 Huang, J., You, Q. L., Panday, A. K., Rupakheti, M., Chen, D. L., Gustafsson, O., Thiemens, M. H.,  
26 and Qin, D. H.: Linking atmospheric pollution to cryospheric change in the Third Pole region:  
27 current progress and future prospects, *Natl Sci Rev*, 6, 796-809, 2019.
- 28 Kishore Kumar, G., Kishore Kumar, K., Baumgarten, G., and Ramkumar, G.: Validation of MERRA  
29 reanalysis upper-level winds over low latitudes with independent rocket sounding data, *J Atmos  
30 Sol-Terr Phys*, 123, 48-54, <https://doi.org/10.1016/j.jastp.2014.12.001>, 2015.
- 31 Li, K., Jacob, D. J., Liao, H., Shen, L., Zhang, Q., and Bates, K. H.: Anthropogenic drivers of 2013–2017  
32 trends in summer surface ozone in China, *Proceedings of the National Academy of Sciences*, 116,  
33 422, 10.1073/pnas.1812168116, 2019.
- 34 Li, K., Jacob, D. J., Shen, L., Lu, X., De Smedt, I., and Liao, H.: Increases in surface ozone pollution in  
35 China from 2013 to 2019: anthropogenic and meteorological influences, *Atmos. Chem. Phys.*, 20,  
36 11423-11433, 10.5194/acp-20-11423-2020, 2020.
- 37 Li, M., Zhang, Q., Kurokawa, J., Woo, J. H., He, K. B., Lu, Z. F., Ohara, T., Song, Y., Streets, D. G.,  
38 Carmichael, G. R., Cheng, Y. F., Hong, C. P., Huo, H., Jiang, X. J., Kang, S. C., Liu, F., Su, H., and  
39 Zheng, B.: MIX: a mosaic Asian anthropogenic emission inventory under the international  
40 collaboration framework of the MICS-Asia and HTAP, *Atmos Chem Phys*, 17, 935-963,  
41 10.5194/acp-17-935-2017, 2017.
- 42 Loewen, M., Kang, S., Armstrong, D., Zhang, Q., Tomy, G., and Wang, F.: Atmospheric transport of  
43 mercury to the Tibetan plateau, *Environmental Science & Technology*, 41, 7632-7638, 2007.
- 44 Lu, X., Hong, J., Zhang, L., Cooper, O. R., Schultz, M. G., Xu, X., Wang, T., Gao, M., Zhao, Y., and



- 1 Zhang, Y.: Severe Surface Ozone Pollution in China: A Global Perspective, *Environ Sci Tech Lett*,  
2 5, 487-494, 10.1021/acs.estlett.8b00366, 2018.
- 3 Lu, X., Zhang, L., Chen, Y., Zhou, M., Zheng, B., Li, K., Liu, Y., Lin, J., Fu, T. M., and Zhang, Q.:  
4 Exploring 2016–2017 surface ozone pollution over China: source contributions and meteorological  
5 influences, *Atmos. Chem. Phys.*, 19, 8339-8361, 10.5194/acp-19-8339-2019, 2019a.
- 6 Lu, X., Zhang, L., and Shen, L.: Meteorology and Climate Influences on Tropospheric Ozone: a Review  
7 of Natural Sources, Chemistry, and Transport Patterns, *Current Pollution Reports*, 5, 238-260,  
8 10.1007/s40726-019-00118-3, 2019b.
- 9 Lu, X., Zhang, L., Wang, X., Gao, M., Li, K., Zhang, Y., Yue, X., and Zhang, Y.: Rapid Increases in  
10 Warm-Season Surface Ozone and Resulting Health Impact in China Since 2013, *Environ Sci Tech*  
11 *Let*, 7, 240-247, 10.1021/acs.estlett.0c00171, 2020.
- 12 Lu, X., Ye, X., Zhou, M., Zhao, Y., Weng, H., Kong, H., Li, K., Gao, M., Zheng, B., Lin, J., Zhou, F.,  
13 Zhang, Q., Wu, D., Zhang, L., and Zhang, Y.: The underappreciated role of agricultural soil nitrogen  
14 oxide emissions in ozone pollution regulation in North China, *Nature Communications*, 12, 5021,  
15 10.1038/s41467-021-25147-9, 2021.
- 16 Lüthi, Z. L., Škerlak, B., Kim, S. W., Lauer, A., Mues, A., Rupakheti, M., and Kang, S.: Atmospheric  
17 brown clouds reach the Tibetan Plateau by crossing the Himalayas, *Atmos. Chem. Phys.*, 15, 6007-  
18 6021, 10.5194/acp-15-6007-2015, 2015.
- 19 Ma, M., Gao, Y., Wang, Y., Zhang, S., Leung, L. R., Liu, C., Wang, S., Zhao, B., Chang, X., Su, H.,  
20 Zhang, T., Sheng, L., Yao, X., and Gao, H.: Substantial ozone enhancement over the North China  
21 Plain from increased biogenic emissions due to heat waves and land cover in summer 2017, *Atmos.*  
22 *Chem. Phys.*, 19, 12195-12207, 10.5194/acp-19-12195-2019, 2019.
- 23 Maione, M., Giostra, U., Arduini, J., Furlani, F., Bonasoni, P., Cristofanelli, P., Laj, P., and Vuillermoz,  
24 E.: Three-year observations of halocarbons at the Nepal Climate Observatory at Pyramid (NCO-P,  
25 5079 m a.s.l.) on the Himalayan range, *Atmos. Chem. Phys.*, 11, 3431-3441, 10.5194/acp-11-3431-  
26 2011, 2011.
- 27 Mustafa, F., Bu, L., Wang, Q., Yao, N., Shahzaman, M., Bilal, M., Aslam, R. W., and Iqbal, R.: Neural-  
28 network-based estimation of regional-scale anthropogenic CO<sub>2</sub> emissions using an Orbiting Carbon  
29 Observatory-2 (OCO-2) dataset over East and West Asia, *Atmos. Meas. Tech.*, 14, 7277-7290,  
30 10.5194/amt-14-7277-2021, 2021.
- 31 Pu, Z. X., Xu, L., and Salomonson, V. V.: MODIS/Terra observed seasonal variations of snow cover over  
32 the Tibetan Plateau, *Geophys Res Lett*, 34, 2007.
- 33 Putero, D., Landi, T. C., Cristofanelli, P., Marinoni, A., Laj, P., Duchi, R., Calzolari, F., Verza, G. P., and  
34 Bonasoni, P.: Influence of open vegetation fires on black carbon and ozone variability in the  
35 southern Himalayas (NCO-P, 5079 m a.s.l.), *Environmental Pollution*, 184, 597-604,  
36 <https://doi.org/10.1016/j.envpol.2013.09.035>, 2014.
- 37 Qiu, J.: The third pole, *Nature*, 454, 393-396, 2008.
- 38 Santer, B. D., Thorne, P. W., Haimberger, L., Taylor, K. E., Wigley, T. M. L., Lanzante, J. R., Solomon,  
39 S., Free, M., Gleckler, P. J., Jones, P. D., Karl, T. R., Klein, S. A., Mears, C., Nychka, D., Schmidt,  
40 G. A., Sherwood, S. C., and Wentz, F. J.: Consistency of modelled and observed temperature trends  
41 in the tropical troposphere, *Int J Climatol*, 28, 1703-1722, 2008.
- 42 Shen, Z., Cao, J., Zhang, L., Zhao, Z., Dong, J., Wang, L., Wang, Q., Li, G., Liu, S., and Zhang, Q.:  
43 Characteristics of surface O<sub>3</sub> over Qinghai Lake area in Northeast Tibetan Plateau, China, *Sci Total*  
44 *Environ*, 500-501, 295-301, <https://doi.org/10.1016/j.scitotenv.2014.08.104>, 2014.



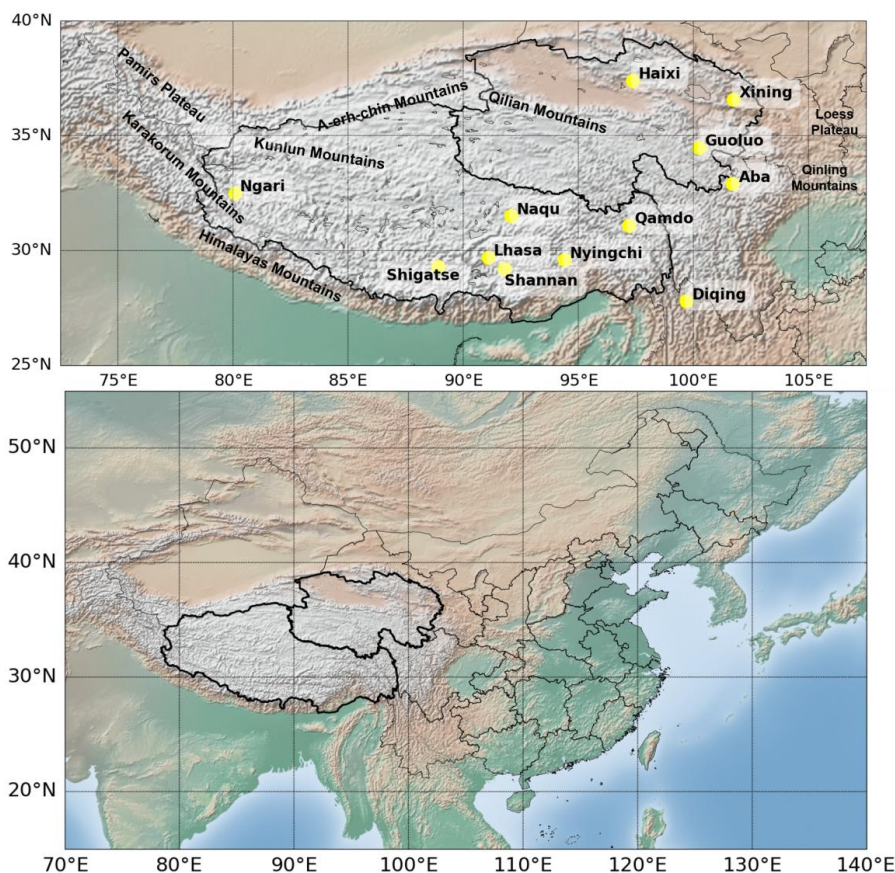
- 1 Shi, Z. B., Song, C. B., Liu, B. W., Lu, G. D., Xu, J. S., Vu, T. V., Elliott, R. J. R., Li, W. J., Bloss, W. J.,  
2 and Harrison, R. M.: Abrupt but smaller than expected changes in surface air quality attributable to  
3 COVID-19 lockdowns, *Sci Adv*, 7, 2021.
- 4 Škerlak, B., Sprenger, M., and Wernli, H.: A global climatology of stratosphere–troposphere exchange  
5 using the ERA-Interim data set from 1979 to 2011, *Atmos. Chem. Phys.*, 14, 913–937, 10.5194/acp-  
6 14-913-2014, 2014.
- 7 Song, Z., Fu, D., Zhang, X., Wu, Y., Xia, X., He, J., Han, X., Zhang, R., and Che, H.: Diurnal and seasonal  
8 variability of PM<sub>2.5</sub> and AOD in North China plain: Comparison of MERRA-2 products and ground  
9 measurements, *Atmos Environ*, 191, 70–78, <https://doi.org/10.1016/j.atmosenv.2018.08.012>, 2018.
- 10 Sun, Y., Wang, Y., and Zhang, C.: Vertical observations and analysis of PM<sub>2.5</sub>, O<sub>3</sub>, and NO<sub>x</sub> at Beijing  
11 and Tianjin from towers during summer and Autumn 2006, *Advances in Atmospheric Sciences*, 27,  
12 123, 10.1007/s00376-009-8154-z, 2009.
- 13 Sun, Y., Liu, C., Zhang, L., Palm, M., Notholt, J., Yin, H., Vigouroux, C., Lutsch, E., Wang, W., Shan,  
14 C., Blumenstock, T., Nagahama, T., Morino, I., Mahieu, E., Strong, K., Langerock, B., De Mazière,  
15 M., Hu, Q., Zhang, H., Petri, C., and Liu, J.: Fourier transform infrared time series of tropospheric  
16 HCN in eastern China: seasonality, interannual variability, and source attribution, *Atmos. Chem.*  
17 *Phys.*, 20, 5437–5456, 10.5194/acp-20-5437-2020, 2020.
- 18 Sun, Y., Yin, H., Liu, C., Mahieu, E., Notholt, J., Té, Y., Lu, X., Palm, M., Wang, W., Shan, C., Hu, Q.,  
19 Qin, M., Tian, Y., and Zheng, B.: The reduction in C<sub>2</sub>H<sub>6</sub> from 2015 to 2020 over Hefei, eastern  
20 China, points to air quality improvement in China, *Atmos. Chem. Phys.*, 21, 11759–11779,  
21 10.5194/acp-21-11759-2021, 2021a.
- 22 Sun, Y., Yin, H., Liu, C., Zhang, L., Cheng, Y., Palm, M., Notholt, J., Lu, X., Vigouroux, C., Zheng, B.,  
23 Wang, W., Jones, N., Shan, C., Qin, M., Tian, Y., Hu, Q., Meng, F., and Liu, J.: Mapping the drivers  
24 of formaldehyde (HCHO) variability from 2015 to 2019 over eastern China: insights from Fourier  
25 transform infrared observation and GEOS-Chem model simulation, *Atmos. Chem. Phys.*, 21, 6365–  
26 6387, 10.5194/acp-21-6365-2021, 2021b.
- 27 Sun, Y., Yin, H., Lu, X., Notholt, J., Palm, M., Liu, C., Tian, Y., and Zheng, B.: The drivers and health  
28 risks of unexpected surface ozone enhancements over the Sichuan Basin, China, in 2020, *Atmos.*  
29 *Chem. Phys.*, 21, 18589–18608, 10.5194/acp-21-18589-2021, 2021c.
- 30 Sun, Y., Yin, H., Cheng, Y., Zhang, Q., Zheng, B., Notholt, J., Lu, X., Liu, C., Tian, Y., and Liu, J.:  
31 Quantifying variability, source, and transport of CO in the urban areas over the Himalayas and  
32 Tibetan Plateau, *Atmos. Chem. Phys.*, 21, 9201–9222, 10.5194/acp-21-9201-2021, 2021d.
- 33 Sun, Y. W., Liu, C., Palm, M., Vigouroux, C., Notholt, J., Hui, Q. H., Jones, N., Wang, W., Su, W. J.,  
34 Zhang, W. Q., Shan, C. G., Tian, Y., Xu, X. W., De Mazière, M., Zhou, M. Q., and Liu, J. G.: Ozone  
35 seasonal evolution and photochemical production regime in the polluted troposphere in eastern  
36 China derived from high-resolution Fourier transform spectrometry (FTS) observations, *Atmos*  
37 *Chem Phys*, 18, 14569–14583, 2018.
- 38 The NASA Global Modeling and Assimilation Office (GMAO),  
39 <https://gmao.gsfc.nasa.gov/reanalysis/MERRA-2/>, last accessed on 1 April, 2022, 2022.
- 40 Vu, T. V., Shi, Z. B., Cheng, J., Zhang, Q., He, K. B., Wang, S. X., and Harrison, R. M.: Assessing the  
41 impact of clean air action on air quality trends in Beijing using a machine learning technique, *Atmos*  
42 *Chem Phys*, 19, 11303–11314, 2019.
- 43 Xu, W. Y., Lin, W. L., Xu, X. B., Tang, J., Huang, J. Q., Wu, H., and Zhang, X. C.: Long-term trends of  
44 surface ozone and its influencing factors at the Mt Waliguan GAW station, China - Part 1: Overall



- 1 trends and characteristics, *Atmos Chem Phys*, 16, 6191-6205, 2016.
- 2 Xue, L. K., Wang, T., Zhang, J. M., Zhang, X. C., Deliger, Poon, C. N., Ding, A. J., Zhou, X. H., Wu, W.  
3 S., Tang, J., Zhang, Q. Z., and Wang, W. X.: Source of surface ozone and reactive nitrogen speciation  
4 at Mount Waliguan in western China: New insights from the 2006 summer study, *Journal of*  
5 *Geophysical Research: Atmospheres*, 116, <https://doi.org/10.1029/2010JD014735>, 2011.
- 6 Yanai, M. H., Li, C. F., and Song, Z. S.: Seasonal Heating of the Tibetan Plateau and Its Effects on the  
7 Evolution of the Asian Summer Monsoon, *J Meteorol Soc Jpn*, 70, 319-351, 1992.
- 8 Yang, R. Q., Zhang, S. J., Li, A., Jiang, G. B., and Jing, C. Y.: Altitudinal and Spatial Signature of  
9 Persistent Organic Pollutants in Soil, Lichen, Conifer Needles, and Bark of the Southeast Tibetan  
10 Plateau: Implications for Sources and Environmental Cycling, *Environmental Science &*  
11 *Technology*, 47, 12736-12743, 2013.
- 12 Yin, H., Sun, Y., Liu, C., Zhang, L., Lu, X., Wang, W., Shan, C., Hu, Q., Tian, Y., Zhang, C., Su, W.,  
13 Zhang, H., Palm, M., Notholt, J., and Liu, J.: FTIR time series of stratospheric NO<sub>2</sub> over Hefei,  
14 China, and comparisons with OMI and GEOS-Chem model data, *Opt Express*, 27, A1225-A1240,  
15 [10.1364/OE.27.0A1225](https://doi.org/10.1364/OE.27.0A1225), 2019a.
- 16 Yin, H., Sun, Y., Liu, C., Lu, X., Smale, D., Blumenstock, T., Nagahama, T., Wang, W., Tian, Y., Hu, Q.,  
17 Shan, C., Zhang, H., and Liu, J.: Ground-based FTIR observation of hydrogen chloride (HCl) over  
18 Hefei, China, and comparisons with GEOS-Chem model data and other ground-based FTIR stations  
19 data, *Opt Express*, 28, 8041-8055, [10.1364/OE.384377](https://doi.org/10.1364/OE.384377), 2020.
- 20 Yin, H., Liu, C., Hu, Q., Liu, T., Wang, S., Gao, M., Xu, S., Zhang, C., and Su, W.: Opposite impact of  
21 emission reduction during the COVID-19 lockdown period on the surface concentrations of PM<sub>2.5</sub>  
22 and O<sub>3</sub> in Wuhan, China, *Environmental Pollution*, 289, 117899,  
23 <https://doi.org/10.1016/j.envpol.2021.117899>, 2021a.
- 24 Yin, H., Lu, X., Sun, Y., Li, K., Gao, M., Zheng, B., and Liu, C.: Unprecedented decline in summertime  
25 surface ozone over eastern China in 2020 comparably attributable to anthropogenic emission  
26 reductions and meteorology, *Environ Res Lett*, 16, 124069, [10.1088/1748-9326/ac3e22](https://doi.org/10.1088/1748-9326/ac3e22), 2021b.
- 27 Yin, H., Sun, Y., Notholt, J., Palm, M., and Liu, C.: Spaceborne tropospheric nitrogen dioxide (NO<sub>2</sub>)  
28 observations from 2005–2020 over the Yangtze River Delta (YRD), China: variabilities,  
29 implications, and drivers, *Atmos. Chem. Phys.*, 22, 4167-4185, [10.5194/acp-22-4167-2022](https://doi.org/10.5194/acp-22-4167-2022), 2022.
- 30 Yin, X., Foy, B. D., Wu, K., Feng, C., and Zhang, Q.: Gaseous and particulate pollutants in Lhasa, Tibet  
31 during 2013–2017: Spatial variability, temporal variations and implications, *Environmental*  
32 *Pollution*, 253, 2019b.
- 33 Yin, X. F., Kang, S. C., de Foy, B., Cong, Z. Y., Luo, J. L., Zhang, L., Ma, Y. M., Zhang, G. S., Rupakheti,  
34 D., and Zhang, Q. G.: Surface ozone at Nam Co in the inland Tibetan Plateau: variation, synthesis  
35 comparison and regional representativeness, *Atmos Chem Phys*, 17, 11293-11311, 2017.
- 36 Yin, X. F., de Foy, B., Wu, K. P., Feng, C., Kang, S. C., and Zhang, Q. G.: Gaseous and particulate  
37 pollutants in Lhasa, Tibet during 2013-2017: Spatial variability, temporal variations and  
38 implications, *Environmental Pollution*, 253, 68-77, 2019c.
- 39 Zhai, S., Jacob, D. J., Wang, X., Shen, L., Li, K., Zhang, Y., Gui, K., Zhao, T., and Liao, H.: Fine  
40 particulate matter (PM<sub>2.5</sub>) trends in China, 2013–2018: separating contributions from anthropogenic  
41 emissions and meteorology, *Atmos. Chem. Phys.*, 19, 11031-11041, [10.5194/acp-19-11031-2019](https://doi.org/10.5194/acp-19-11031-2019),  
42 2019.
- 43 Zhang, Y. M., Vu, T. V., Sun, J. Y., He, J. J., Shen, X. J., Lin, W. L., Zhang, X. Y., Zhong, J. T., Gao, W.  
44 K., Wang, Y. Q., Fu, T. Y., Ma, Y. P., Li, W. J., and Shi, Z. B.: Significant Changes in Chemistry of



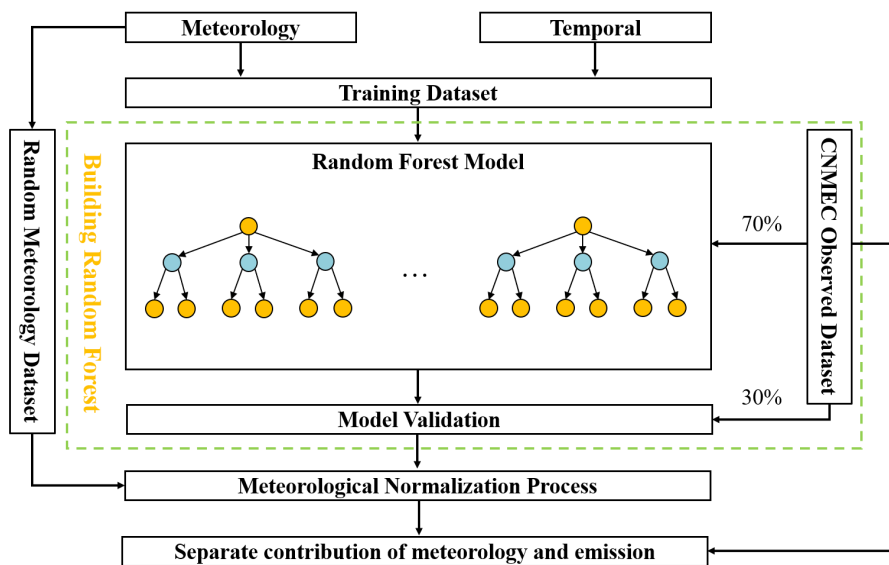
- 1 Fine Particles in Wintertime Beijing from 2007 to 2017: Impact of Clean Air Actions,  
2 Environmental Science & Technology, 54, 1344-1352, 2020.
- 3 Zhao, S. P., Yu, Y., Yin, D. Y., He, J. J., Liu, N., Qu, J. J., and Xiao, J. H.: Annual and diurnal variations  
4 of gaseous and particulate pollutants in 31 provincial capital cities based on in situ air quality  
5 monitoring data from China National Environmental Monitoring Center, Environment International,  
6 86, 92-106, 2016.
- 7 Zhou, C., Wang, K., and Ma, Q.: Evaluation of Eight Current Reanalyses in Simulating Land Surface  
8 Temperature from 1979 to 2003 in China, J Climate, 30, 7379-7398, 10.1175/JCLI-D-16-0903.1,  
9 2017.
- 10 Zhu, B., Akimoto, H., Wang, Z., Sudo, K., Tang, J., and Uno, I.: Why does surface ozone peak in  
11 summertime at Waliguan?, Geophys Res Lett, 31, 2004.
- 12 Zhu, N. L., Fu, J. J., Gao, Y., Ssebugere, P., Wang, Y. W., and Jiang, G. B.: Hexabromocyclododecane in  
13 alpine fish from the Tibetan Plateau, China, Environmental Pollution, 181, 7-13, 2013.
- 14  
15



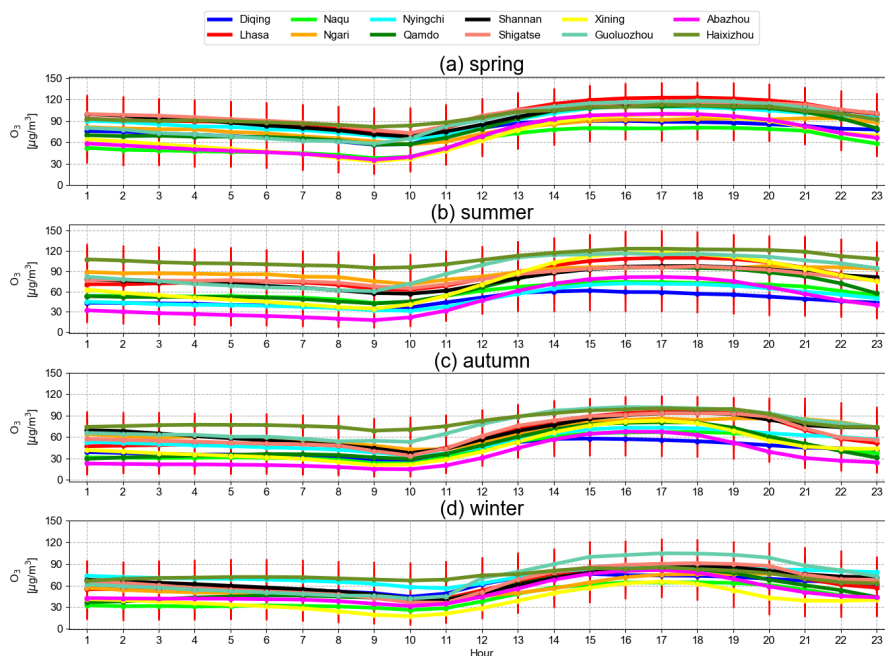
1  
2 **Figure 1.** Geolocations of each city over the Qinghai-Tibet Plateau (QTP). The base map of the  
3 figure was created using the Basemap package in Python.

4

5

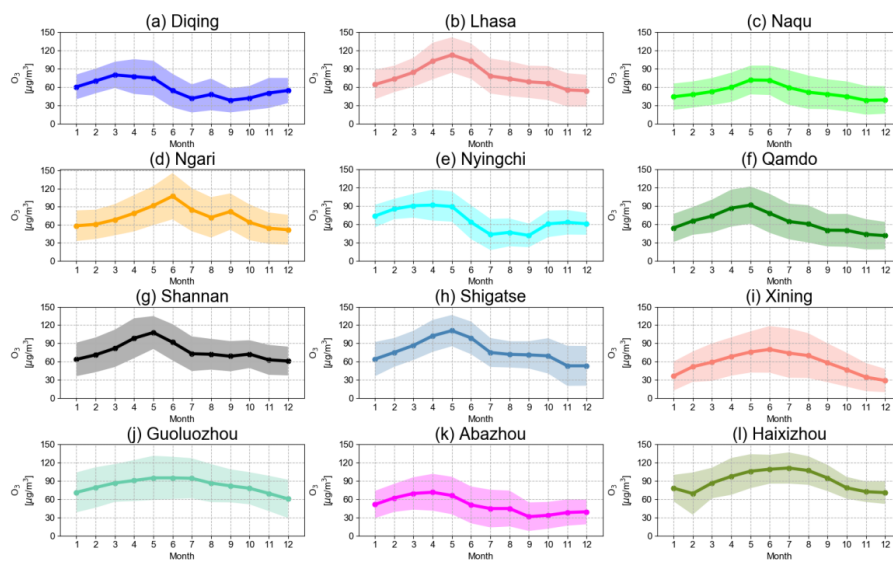


1  
2 **Figure 2.** Flowchart for separation of meteorology and anthropologic contributions.  
3



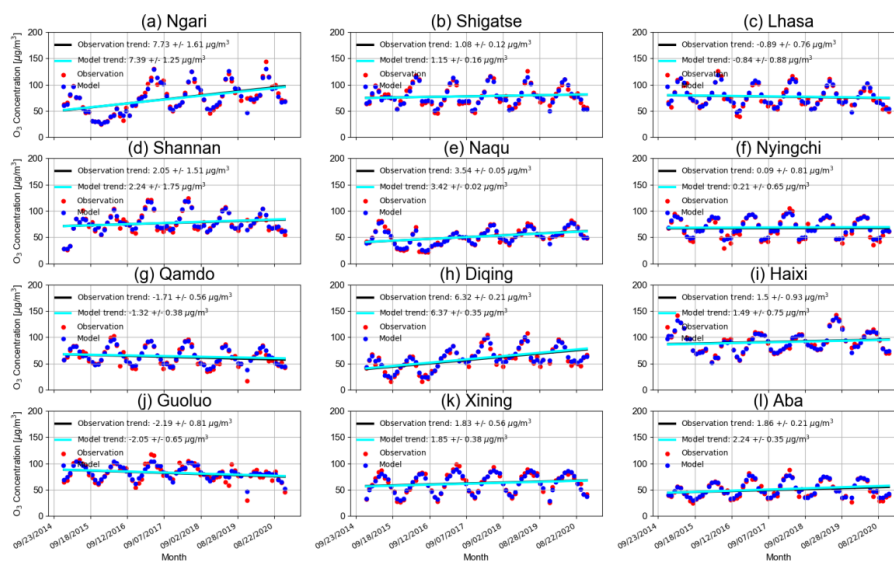
1  
2  
3  
4

**Figure 3.** Diurnal cycle of surface ozone (units:  $\mu\text{g}/\text{m}^3$ ) in each season and each city over the QTP. The vertical error bar is  $1\sigma$  standard variation (STD) within that hour.

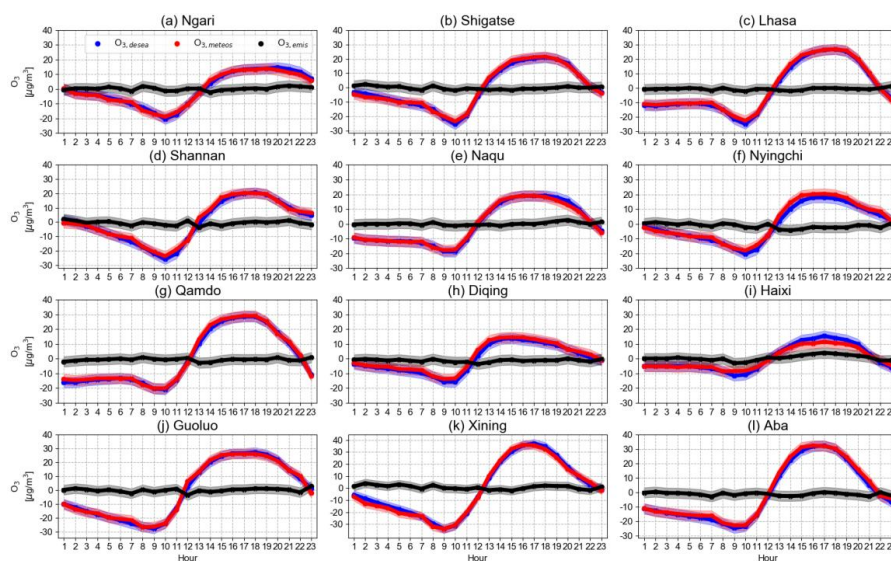


1  
2 **Figure 4.** Monthly mean time series of surface ozone (units:  $\mu\text{g}/\text{m}^3$ ) between 2015 and 2020 in each  
3 city over the QTP. The vertical error bar is  $1\sigma$  standard variation (STD) within that month.

4

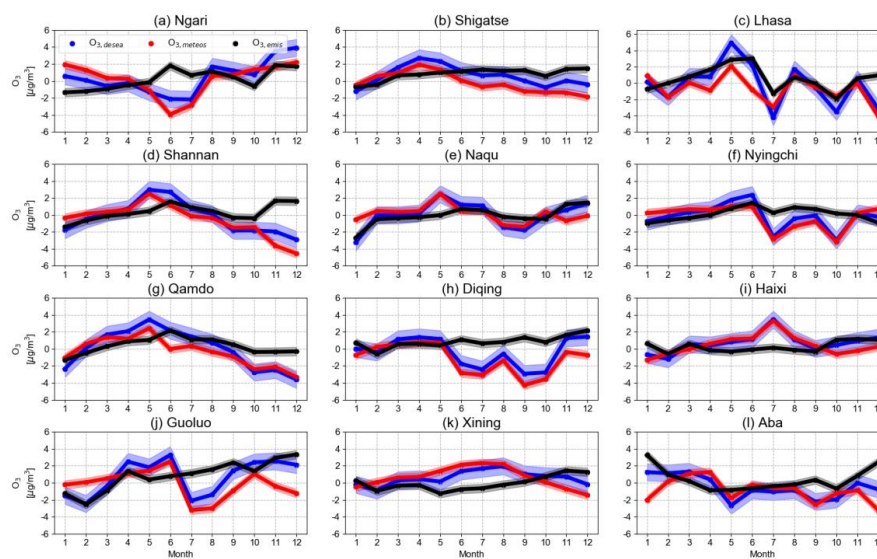


1  
2 **Figure 5.** Inter-annual trends of surface ozone levels between 2015 and 2020 in the urban areas over  
3 the QTP. Blue dots are the monthly averaged surface ozone measurements. The seasonality and  
4 inter-annual variability in each city fitted by using a bootstrap resampling model with a second  
5 Fourier series (red dots) plus a linear function (black line) is also shown.  
6

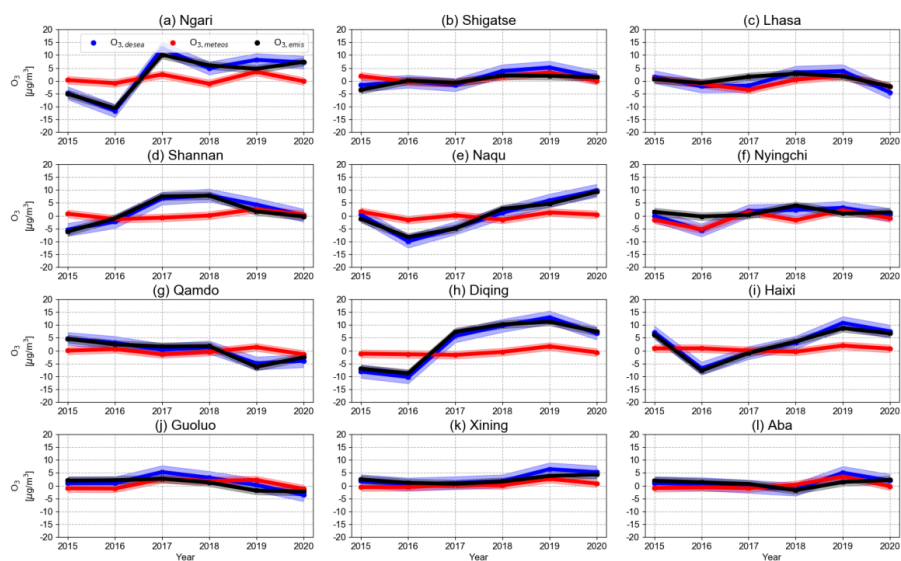


1  
2 **Figure 6.** Diurnal cycles of surface ozone anomalies ( $O_{3,anomalies}$ , blue dots and lines) along with  
3 the meteorology-driven portions ( $O_{3,meteo}$ , red dots and lines) and the anthropogenic-driven  
4 portions ( $O_{3,emis}$ , black dots and lines) in each city over the QTP. Bold curves and the shadows are  
5 diurnal cycles and the  $1\sigma$  standard variations, respectively.

6



1  
2 **Figure 7.** Seasonal cycles of surface ozone anomalies ( $O_{3,anomalies}$ , blue dots and lines) along with  
3 the meteorology-driven portions ( $O_{3,meteo}$ , red dots and lines) and the anthropogenic-driven  
4 portions ( $O_{3,emis}$ , black dots and lines) in each city over the QTP. Bold curves and the shadows are  
5 monthly mean values and the  $1\sigma$  standard variations, respectively.  
6



1  
2 **Figure 8.** Annual mean surface ozone anomalies ( $O_{3,anomalies}$ , blue dots and lines) along with  
3 meteorology-driven portions ( $O_{3,meteo}$ , red dots and lines) and anthropogenic-driven portions  
4 ( $O_{3,emis}$ , black dots and lines) in each city over the QTP. Bold curves and the shadows are annual  
5 mean values and the  $1\sigma$  standard variations, respectively.  
6



1 **Table 1.** Geolocations of each city over the QTP. Population statistics are available from the 2020  
2 nationwide population census issued by National Bureau of Statistics of China.

Name	Latitude	Longitude	Number of site	Altitude (km)	Population (million)	Area (Thousand km <sup>2</sup> )
Ngari	32.5°N	80.1°E	2	4.5	0.12	345.0
Shigatse	29.3°N	88.9°E	3	4.0	0.80	182.0
Lhasa	29.7°N	91.1°E	6	3.7	0.87	31.7
Shannan	29.2°N	91.8°E	2	3.7	0.35	79.3
Naqu	31.5°N	92.1°E	3	4.5	0.50	430.0
Nyingchi	29.6°N	94.4°E	2	3.1	0.23	117.0
Qamdo	31.1°N	97.2°E	3	3.4	0.76	110.0
Diqing	27.8°N	99.7°E	2	3.5	0.39	23.9
Haixi	37.4°N	97.4°E	1	4.8	0.47	325.8
Guoluo	34.5°N	100.3°E	1	4.3	0.21	76.4
Xining	36.6°N	101.7°E	5	2.3	2.47	7.7
Aba	32.9°N	101.7°E	3	3.8	0.82	84.2

3

4



1 **Table 2.** List of predictive variables fed into the RF model.

Parameters	Description	Unit
Meteorological variables by MERRA-2 dataset		
T <sub>surface</sub>	Surface air temperature	°C
U <sub>10m</sub>	zonal wind at 10 m height	m/s
V <sub>10m</sub>	meridional wind at 10 m height	m/s
PBLH	Planetary boundary layer height	m
CLDT	Total cloud area fraction	unitless
PRECTOT	Total Precipitation	kg·m <sup>2</sup> /s
OMEGA	Vertical pressure velocity at PBLH	Pa/s
SWGDN	Surface incoming shortwave flux	W/m <sup>2</sup>
QV	Specific humidity at 2 m height	kg/kg
TROPT	Tropospheric layer pressure	Pa
Time information		
Year	Year since 2015	/
Month	Month of the year	/
day	Day of the month	/
Hour	Hour of the day	/

2